Article

Delayed Coupling to Feedback Inhibition during a Critical Period for the Integration of Adult-Born Granule Cells

Highlights

- Developing GCs transition from weak to strong coupling to feedback inhibition

- Mature but not young GCs activate dentate gyrus PV interneurons in vivo

- Feedback inhibition by mature GCs contributes to sparse coding

- A computational model reveals developing GCs crucial for input discrimination

Authors

Silvio G. Temprana, Lucas A. Mongiat, ...,
Guillermo M. Lanuza,
Alejandro F. Schinder

Correspondence

aschinder@leloir.org.ar

In Brief

Temprana et al. show that immature adult-born granule cells activate CA3 networks but that they are poorly coupled to feedback inhibition. As neurons mature, they recruit strong inhibitory loops that restrict spiking, promoting sparse activity in the granule cell layer.

CrossMark

CellPress

Delayed Coupling to Feedback Inhibition during a Critical Period for the Integration of Adult-Born Granule Cells

Silvio G. Temprana,[1,3] Lucas A. Mongiat,[1,3] Sung M. Yang,[1,3] Mariela F. Trinchero,[1] Diego D. Alvarez,[1] Emilio Kropff,[1] Damiana Giacomini,[1] Natalia Beltramone,[1] Guillermo M. Lanuza,[2] and Alejandro F. Schinder[1,*]
[1]Laboratory of Neuronal Plasticity
[2]Laboratory of Developmental Neurobiology
Leloir Institute–CONICET, Av. Patricias Argentinas 435, Buenos Aires, C1405BWE, Argentina
[3]Co-first authors
*Correspondence: aschinder@leloir.org.ar
http://dx.doi.org/10.1016/j.neuron.2014.11.023

SUMMARY

Developing granule cells (GCs) of the adult dentate gyrus undergo a critical period of enhanced activity and synaptic plasticity before becoming mature. The impact of developing GCs on the activity of preexisting dentate circuits remains unknown. Here we combine optogenetics, acute slice electrophysiology, and in vivo chemogenetics to activate GCs at different stages of maturation to study the recruitment of local target networks. We show that immature (4-week-old) GCs can efficiently drive distal CA3 targets but poorly activate proximal interneurons responsible for feedback inhibition (FBI). As new GCs transition toward maturity, they reliably recruit GABAergic feedback loops that restrict spiking of neighbor GCs, a mechanism that would promote sparse coding. Such inhibitory loop impinges only weakly in new cohorts of young GCs. A computational model reveals that the delayed coupling of new GCs to FBI could be crucial to achieve a fine-grain representation of novel inputs in the dentate gyrus.

INTRODUCTION

The majority of adult neural circuits rely on activity-dependent synaptic modification as a primary mechanism for experience-induced plasticity, which is central to adaptive behavior and learning (Caroni et al., 2012; Holtmaat and Svoboda, 2009). The dentate gyrus of the hippocampus is a cortical structure involved in memory encoding that, in addition to synaptic plasticity, relies on the continuous generation of new dentate granule cells (GCs) throughout life. GCs, the principal neurons of the dentate gyrus, assemble the granule cell layer (GCL) that is characterized by its sparse activity (Chawla et al., 2005). They receive primarily excitatory projections from the entorhinal cortex and inhibitory inputs from local interneurons. Their axons (mossy fibers) contact GABAergic interneurons, hilar mossy cells, and pyramidal cells located in the CA3 pyramidal layer (Acsády et al., 1998; Freund and Buzsáki, 1996; Henze et al., 2002). The roles of the individual players of these local networks in memory encoding are still poorly understood.

Adult-born GCs develop over several weeks, displaying slow morphological and functional maturation, also regulated in an activity-dependent manner (Chancey et al., 2013; Espósito et al., 2005; Ge et al., 2006; Overstreet-Wadiche et al., 2006; Piatti et al., 2011). New GCs become functionally integrated within the pre-existing circuits and participate in information processing (Ming and Song, 2011; Mongiat and Schinder, 2011; Piatti et al., 2013; van Praag et al., 2002; Zhao et al., 2008). In vivo studies monitoring expression of immediate early genes have shown that adult-born GCs are activated by spatial learning (Ramirez-Amaya et al., 2006; Stone et al., 2011; Trouche et al., 2009). In addition, accumulating evidence has indicated that modifying the extent of adult neurogenesis substantially alters the animal's ability to perform specific learning tasks, primarily those involving behavioral pattern separation (Clelland et al., 2009; Creer et al., 2010; Dupret et al., 2008; Nakashiba et al., 2012; Sahay et al., 2011). While the relevance of neurogenesis in hippocampal function has been validated, the precise contribution of adult-born neurons to circuit plasticity and, consequently, information processing, is still unclear.

In recent years much of the discussion in the field has centered on the notion that immature adult-born neurons may be of particular relevance to information processing in the dentate gyrus due to their high excitability and plasticity, a concept established both from physiology and from behavioral data. GCs become mature after developing for 6–8 weeks, at which time they are both morphologically and functionally very similar to GCs born during perinatal development; they receive excitatory inputs from the medial and lateral entorhinal cortex and inhibitory inputs from local interneurons including parvalbumin^{+} cells, somatostatin^{+} cells, HICAP cells, MOPP cells, and neurogliaform cells (Deshpande et al., 2013; Laplagne et al., 2006; Li et al., 2013; Markwardt et al., 2009, 2011; Vivar et al., 2012). Their axons (mossy fibers) synapse onto typical GC targets, which include hilar interneurons, CA3 interneurons, and pyramidal cells (Faulkner et al., 2008; Gu et al., 2012; Toni et al., 2008). Interestingly,

4-week-old GCs are morphologically and functionally immature, but they may already process information: they integrate synaptic inputs, spike, and release glutamate onto target cells (Gu et al., 2012; Marín-Burgin et al., 2012; Mongiat et al., 2009; Stone et al., 2011). They also display enhanced activity-dependent potentiation in their excitatory input and output synapses, making them efficient substrates of hebbian plasticity (Ge et al., 2007; Gu et al., 2012; Schmidt-Hieber et al., 2004; Snyder et al., 2001). Moreover, a delay in the establishment of mature perisomatic inhibition results in a high excitation/inhibition balance that confers immature GC low activation threshold and low input specificity, consequently becoming a highly active neuronal population that is immersed within a principal layer (the GCL) characterized by sparse activity (Dieni et al., 2013; Espósito et al., 2005; Marín-Burgin et al., 2012; Piatti et al., 2013; Song et al., 2013). A puzzling question then emerges directly from those findings: do young GCs with low input specificity contribute to dentate gyrus function? To address this problem it is important to define the developmental stage at which new GCs become functionally relevant to the local networks in a manner that can influence information processing (i.e., alter input/output properties in the dentate). We reasoned that the specific function of adult-born GCs might be better understood after identifying the local networks they recruit along their transition from immature to fully mature, which has remained unknown.

Here we have addressed a set of simple questions to test the hypothesis that activation of immature versus mature adult-born GCs would recruit distinct postsynaptic targets cells and networks, and thus impinge differentially on the activity of the principal layers. We show that output networks switch as GCs mature. Most remarkably, immature GCs exert poor feedback control over their neighbor neurons. Upon maturation, mossy fibers recruit proximal interneurons responsible for feedback inhibition (FBI) capable of attenuating GCL activity. Our data reveal that immature GCs are poorly coupled to GABAergic inhibition at a time that is coincident with the critical period of low activation threshold and enhanced synaptic plasticity. Remarkably, as GCs mature (and exit the critical period), they begin to recruit and respond to inhibitory feedback. We present a computational model that supports the notion that the delayed coupling to FBI in adult-born GCs provides an efficient mechanism for input discrimination in the dentate gyrus.

RESULTS

The GCL comprises a heterogeneous population of GCs generated at different times from development to adulthood, with more than 80% of the GCs generated postnatally (Altman and Bayer, 1990; Mathews et al., 2010). Hence, understanding the impact of dentate gyrus (DG) activity requires dissecting the output of those distinct neuronal populations. We have considered three major populations of principal neurons: mature GCs generated during adulthood, newly generated young (immature) GCs, and GCs generated during early postnatal development (see Figure S1A available online). In this study, young GCs correspond to 4-week-old neurons, whereas mature GCs are >7 weeks old.

Optogenetic Stimulation of GCs Generated during Early Postnatal Development Recruit Feedforward and Feedback Loops

To characterize the local circuits activated by GCs generated during early postnatal development, we selectively expressed the light-activated channel channelrhodopsin-2 (ChR2) in GCs generated in the early postnatal DG and analyzed their output during adulthood. We utilized Ascl1^{CreERT2};CAG^{floxStopChR2} mice to allow indelible targeting of ChR2 in Ascl1-expressing neural progenitor cells and performed tamoxifen (TAM) induction at postnatal day 11 (P11), thus rendering ChR2 expression in GCs generated from P11 onward (Kim et al., 2007; Madisen et al., 2012). Electrophysiological recordings in acute slices were performed 9 weeks later (Figures 1A and 1B). Due to the pronounced decrease in DG neurogenesis that occurs during early postnatal life (Mathews et al., 2010), the neuronal population expressing ChR2 is greatly enriched in GCs generated around the time of TAM induction. In agreement with this notion, the majority of ChR2-expressing GCs (ChR2-GCs) expressed the neuronal marker calbindin and displayed mature GC morphology with complex spiny dendrites extending through the molecular layer and axons projecting through the hilus reaching the distal CA3 pyramidal layer (Figures 1C and S1B).

The output of this population enriched in mature ChR2-GCs generated during postnatal development was assessed by stimulation using brief (1 ms) blue laser pulses delivered through the microscope objective. Light stimulation triggered action potentials in ChR2-GCs with high efficacy (1 spike/pulse, Figure 1D). To monitor light-evoked synaptic responses, whole-cell recordings were performed in CA3 pyramidal cells under conditions that allowed discriminating excitatory and inhibitory postsynaptic currents (EPSCs and IPSCs) as inward (negative) or outward (positive) deflections (Figure 1E). In voltage-clamp recordings obtained at depolarized holding potentials (~0 mV, the reversal potential for glutamatergic responses), light-mediated ChR2-GC stimulation reliably elicited IPSCs that were blocked by either the GABA$_A$-receptor antagonist picrotoxin (PTX) or by the AMPA/NMDA glutamatergic antagonist kynurenic acid (KYN). This result indicates that IPSCs depend both on glutamate and GABA release, consistent with a feedforward inhibitory (FFI) loop ChR2-GC → GABA interneuron → pyramidal cell (Figures 1E, 1F1, 1F2, and 1F4). In recordings obtained at negative holding potentials (~−70 mV, the reversal potential for GABAergic responses), light-mediated ChR2-GC stimulation reliably elicited EPSCs that were blocked by KYN, but not PTX, reflecting the canonical mossy fiber-CA3 glutamatergic connection that carries dentate output to the CA3 pyramidal layer (Figures 1E, 1F3, and 1F4).

We then performed whole-cell recordings in unlabeled mature GCs located in the outer third of the GCL, primarily generated during development (Marín-Burgin et al., 2012; Mathews et al., 2010). Stimulation of ChR2-GCs elicited IPSCs that were also blocked by either KYN or PTX, now revealing the disynaptic feedback loop ChR2-GC → GABA interneuron → GC (Figures 1G and 1H1–1H3). No feedback excitatory responses were found. These results identify feedback and feedforward interneurons as well as CA3 pyramidal cells as targets of a neuronal
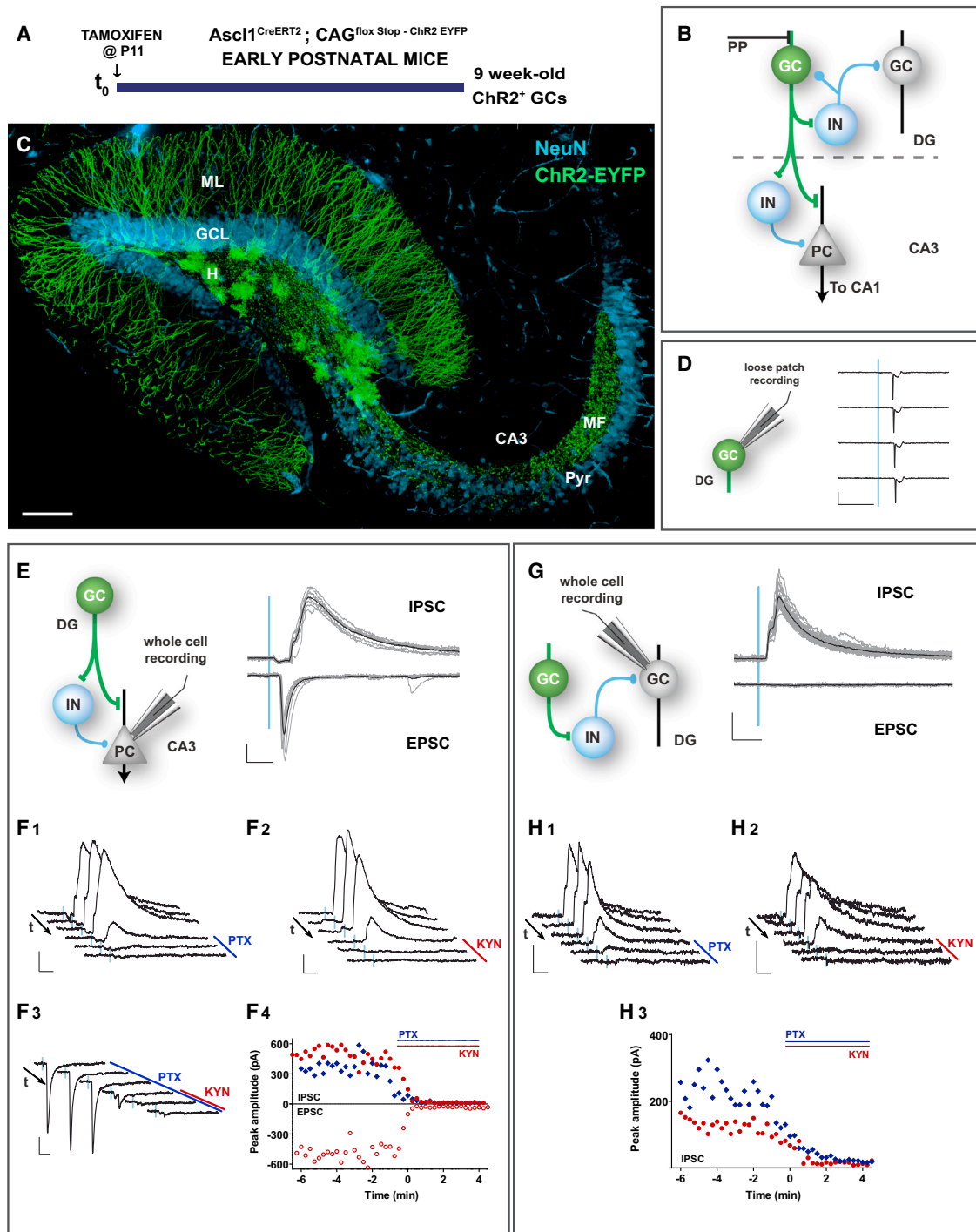
Figure 1. Dentate and CA3 Networks Recruited by GCs Generated during Development

(A) Experimental design. $Ascl1^{CreERT2};CAG^{floxStopChR2}$ mice received TAM injections at P11 to induce indelible expression of ChR2 in neural progenitor cells and were sacrificed 9 weeks later to perform electrophysiological recordings in acute slices. See also Figure S1B.

(B) Simplified diagram of the local dentate networks. ChR2-GCs (green) contact multiple hilar interneurons (IN), CA3 pyramidal cells (PC), and CA3 IN. PP, Perforant path axons.

(C) Confocal image of a 400 μm thick hippocampal section depicting 9-week-old GCs (green) generated at P11. NeuN immunofluorescence (blue) allows visualizing the GCL and CA3 pyramidal layer (pyr). Dendrites extend through the molecular layer (ML); mossy fibers (MF) project through the hilus (H) and to CA3 through the stratum lucidum. Scale, 100 μm.

(D) Loose patch recordings in ChR2-GCs show reliable spiking evoked by a 1 ms laser pulse (denoted by the blue line). Representative data from n = 6 GCs.

(legend continued on next page)

population enriched in mature GCs generated during early postnatal development.

Immature Adult-Born GCs Activate CA3 Networks but Poorly Recruit Inhibitory Feedback Loops

To map the networks activated by adult-born neurons, we selectively expressed ChR2 by retroviral transduction of neural progenitor cells of the adult DG. A retrovirus expressing ChR2-EGFP was delivered to the DG of adult mice, and acute slices were prepared 4 or 7 weeks postinjection (wpi), revealing substantial numbers of ChR2-GCs at both time points (Figures 2A and 2B). Network activation by light-induced stimulation of 4- (young) or 7-week-old (mature) GCs was compared in electrophysiological recordings (Figure 2C). First, loose patch recordings were carried out to measure the reliability of brief (1 ms) laser pulses to induce spiking. In both young and mature ChR2-GCs, light pulses triggered spikes with similar efficacy (about 1 spike/light pulse, Figure 2D) and latency (<4 ms; Figure S2A). We then investigated the CA3 networks recruited by adult-born ChR2-GCs by means of whole-cell recordings in pyramidal cells. In voltage-clamp recordings obtained at 0 mV, laser-mediated stimulation of both young and mature ChR2-GCs elicited GABAergic IPSCs with similar kinetics and synaptic charge (Figures 2E, 2H, and S2A). Although IPSC charge was somewhat larger for mature ChR2-GCs, such increase was minor compared to what is described below for FBI. In recordings obtained at negative holding potentials (−70 mV), optogenetic stimulation elicited glutamatergic EPSCs that also displayed similar kinetics and synaptic charge for both young and mature ChR2-GCs (Figures 2E, 2I, and S2A). EPSCs and IPSCs were completely blocked by the AMPA-subtype glutamate receptor antagonist NBQX (Figure 2G, upper and middle panels), revealing the presence of excitation (mossy fiber → pyramidal cell contacts) and feedforward GABAergic inhibition (ChR2-GC → GABA interneuron → pyramidal cell) pathways onto the CA3 principal layer, similarly to what was described above for mature GCs generated during early postnatal development. These results indicate that although 4 wpi adult-born GCs are still immature, they have already established reliable output connectivity within the CA3 region.

To interrogate the local networks activated by proximal (hilar) mossy fiber contacts, whole-cell recordings were performed in unlabeled mature GCs located in the outer third of the GCL. Laser stimulation of mature adult-born ChR2-GCs elicited reliable IPSCs on neighboring GCs (Figure 2F). IPSCs were fully blocked by NBQX, which reveals that responses correspond to a feedback inhibitory loop ChR2-GC → GABA interneuron →

GC (Figure 2G bottom panel). In striking contrast, laser stimulation of young ChR2-GCs elicited small IPSCs on neighbor GCs, revealing a poor recruitment of FBI (Figures 2F and 2J). Such weak responses were the consequence of the combined effects of small amplitude and low success probability of IPSCs (Figure S2A). Note that the increase in IPSC charge corresponding to FBI from 4 to 8 wpi is about 4-fold the change observed for FFI described above. Thus, adult-born GCs establish distal synapses onto CA3 interneurons and pyramidal cells that are largely developed by 4 wpi, while functional connectivity of proximal mossy fiber contacts responsible for FBI onto the GCL is delayed.

We also tested the ability of young and mature adult-born GCs to exert FBI during patterns of activity that resemble those occurring during hippocampus-dependent behaviors (Leutgeb et al., 2007). ChR2-GCs were stimulated in the range of theta frequency (10 Hz pulses), and whole-cell recordings were performed in unlabeled mature GCs of the external GCL (Figure S2B). Interestingly, the strong inhibitory feedback recruited by mature GCs showed substantial depression, whereas immature GCs activated a small but persistent inhibition, suggesting a differential degree of short-term plasticity within this feedback loop (Torborg et al., 2010).

Feedback Inhibition by Adult-Born Mature GCs Controls Activity of the Principal Layer

To determine the functional relevance of the GABAergic feedback loops recruited by adult-born GCs, we performed recordings of field excitatory postsynaptic potential (fEPSP) in the GCL to monitor the population spike (pop-spike) evoked by stimulation of the medial perforant path (mPP), a primary excitatory input to the DG. The pop-spike area reflects the number of GCs that spike synchronously to the input stimulus. Slices bearing young or mature adult-born ChR2-GCs received a brief pulse of blue light (2 ms) that was paired to the mPP stimulus to recruit FBI and measure its impact on the pop-spike amplitude (Figures 3A–3C). A single light prepulse delivered to mature ChR2-GCs was sufficient to greatly reduce (by ∼40%) mPP-induced pop-spike amplitude in a reliable and reversible manner (Figures 3C, 3E, and 3F). Pop-spike reduction was maximal when the light preceded mPP activation by 10 ms ("−10 ms," Figure 3C), which is coincident with the onset timing of FBI (Figure S2A). Pop-spike area displayed little change when stimulation was delivered to young ChR2-GCs, consistent with the poor recruitment of FBI observed for immature GCs (Figures 3D and 3F). The reduction of pop-spike amplitude elicited by pairing mature ChR2-GC activation to mPP stimulation was

---

(E) Example whole-cell voltage clamp recordings in a PC. (Left) Simplified scheme depicting light-activated pathways. (Right) Brief (1 ms) light pulses delivered at low frequency (0.07 Hz) elicit inhibitory postsynaptic currents (IPSCs, recorded at 0 mV, upper traces) and excitatory postsynaptic currents (EPSCs, recorded at −70 mV, lower traces), recorded in the same neuron. Traces depict all sweeps in the experiment (gray) and their average (black). All cells showed light-evoked PSCs, with IPSC charge = 5.3 ± 2.0 pC, and EPSC charge = 1.9 ± 1.1 pC (n = 5 IPSC, n = 4 EPSC).

(F) (F1–F4) Pharmacological blockade of light-evoked PSCs. Example subsequent traces show IPSCs blockade after bath application of PTX (100 μM, F1) or KYN (6 mM, F2), consistent with a disynaptic FFI response. EPSCs are blocked by KYN (F3). Arrows indicate time flow, and bars denote antagonist application. (F4) Time course of EPSC and IPSC peak amplitude obtained from experiments shown in (F1)–(F3). Drug application for each case is indicated by the colored bars.

(G) Voltage clamp recordings in mature (unlabeled) GCs. (Left) Simplified scheme depicting light-activated pathways. (Right) Single laser pulses (0.07 Hz) elicited IPSCs (upper traces, 100% of trials), but not EPSCs (0% of trials), with IPSC charge = 1.7 ± 0.9 pC, n = 8 GCs.

(H) (H1–H3) Pharmacological blockade of PSCs. Example subsequent traces show IPSCs blockade by PTX (100 μM, H1) or KYN (6 mM, H2), consistent with a disynaptic feedback response. (H3) Time course of IPSC peak amplitude obtained from experiments shown in (H1) and (H2). Scale bars, 20 ms, 100 pA.
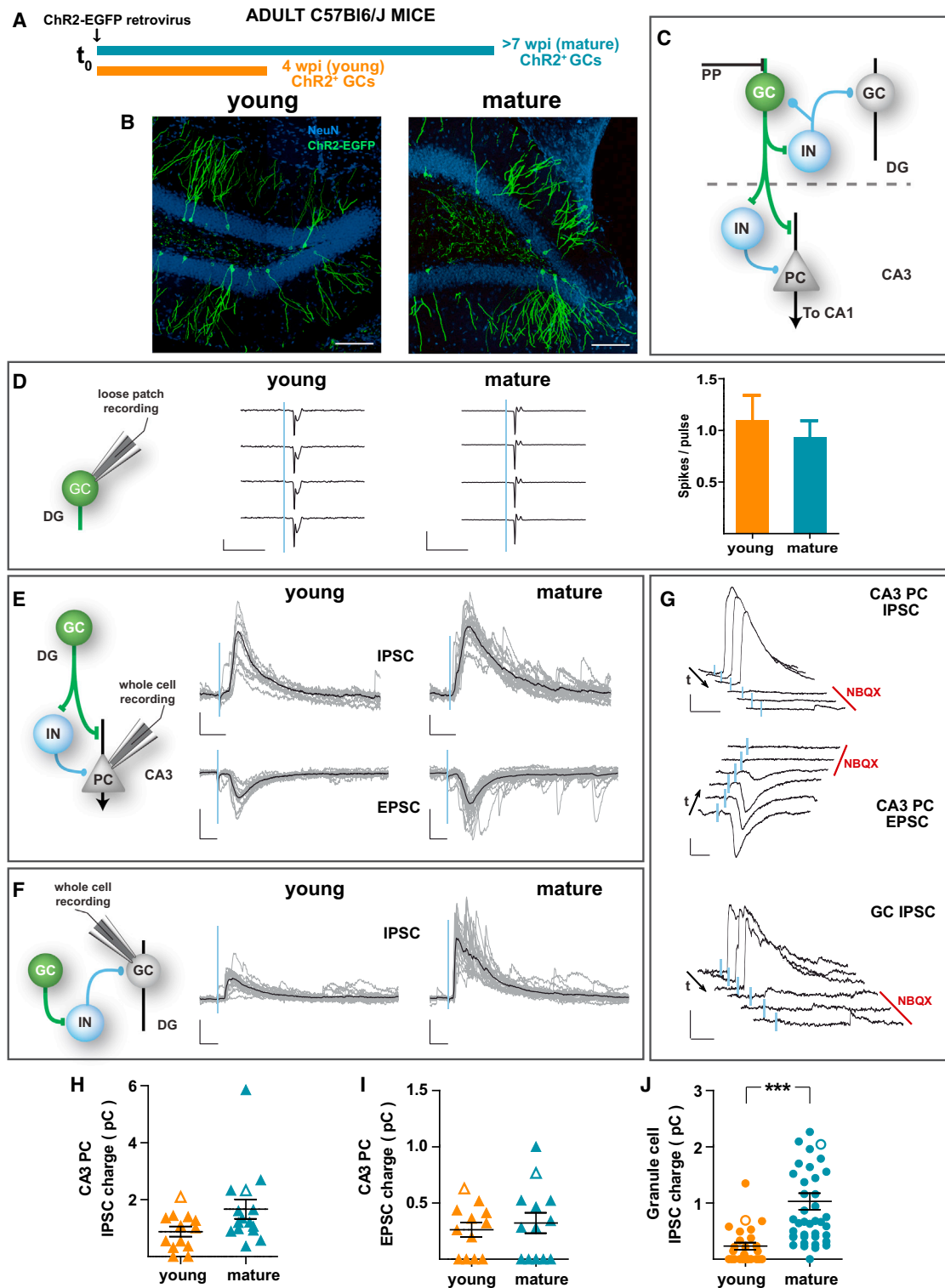
Figure 2. Distinct Local Networks Recruited by Immature versus Mature Adult-Born GCs

(A) Experimental design. A retrovirus encoding for ChR2-EGFP was delivered to the DG of young adult mice. Acute slices were obtained 4 (orange) or 7 (blue) weeks later for electrophysiological recordings.

(B) Confocal images displaying adult-born young and mature ChR2-GCs (green). NeuN (blue) allows visualization of the GCL. Calibration bar, 100 μm.

(C) Simplified diagram of the local dentate networks. ChR2-GCs (green) contact multiple hilar interneurons (IN), CA3 pyramidal cells (PC), and CA3 IN. PP, perforant path axons.

(legend continued on next page)

blocked by PTX, indicating that the effect was mediated by the recruitment of feedback GABAergic inhibition (Figure 3G).

In addition, whole-cell recordings indicated that light-evoked FBI by mature GCs was sufficient to induce a substantial reduction of the excitation/inhibition balance during the phase of signal integration (Figure S3), consistent with the observed reduction in spiking probability. Interestingly, light-mediated recruitment of FBI did not alter the fEPSP slope, which accounts for the magnitude of dendritic synaptic depolarization (Figure 3F). Therefore, it is likely that FBI reduces spiking without modifying the excitatory synaptic gain (consistent with a perisomatic action) or, alternatively, that the reduction in fEPSP may be masked by the shunting depolarization exerted by GABA in GCs (Andersen et al., 2007; Chiang et al., 2012; Sauer et al., 2012). These results demonstrate that activation of few mature adult-born GCs can greatly restrict the size of the spiking population, thus contributing to the sparse activation of the GCL.

Immature GCs Receive Weak FBI

Mature GCs impose a powerful inhibitory loop that controls GCL spiking (Figures 2 and 3). We asked if all principal neurons in the GCL are under control of such feedback loop, in particular immature GCs, which, as we previously demonstrated, lack functional perisomatic GABAergic inhibition (Espósito et al., 2005; Marín-Burgin et al., 2012). To address this question, we utilized retroviral delivery of ChR2 to obtain ChR2-GCs in GLAST[CreERT2]; CAG[FloxStopTom] mice (Madisen et al., 2010; Mori et al., 2006). Three weeks later we injected TAM to induce Cre-mediated labeling in new GCs (Tom-GCs). Electrophysiological recordings in acute slices were performed 4 weeks later (Figures 4A and 4B). Thus, Tom-GCs corresponded to young GCs that displayed functional and morphological properties typical of immature adult-born GCs (Figure S4A), while ChR2-GCs corresponded to mature GCs at 7 wpi. Whole-cell recordings were carried out alternately in Tom-GCs and in mature unlabeled GCs from the outer GCL to compare their synaptic inputs in the same slices (Figure 4C). Light stimulation of mature ChR2-GCs reliably elicited strong IPSCs in mature GCs and weaker responses in immature Tom-GCs (Figures 4C, 4D, and S4B). Moreover, in a similar set of experiments in which both ChR2-GCs and Tom-GCs were 4 wpi, weak postsynaptic responses were recorded in young and mature GCs (Figure S4C). Thus, in spite of the overall strong FBI reaching the GCL recruited by mature GCs, inhibitory feedback exerts only limited modulation on the activity of young GCs.

Activation of Mature GCs In Vivo Recruit Parvalbumin[+] GABAergic Interneurons

The experiments described above reveal critical differences in regard to the feedback loops recruited by immature and mature GCs, and to the actions of those loops onto the distinct neuronal populations that build the GCL. We then designed an experiment to monitor whether the activity of adult-born GCs may differentially activate local networks in vivo. We utilized retroviral delivery of the hM3Dq synthetic G-coupled receptor (Alexander et al., 2009) to activate adult-born GCs upon administration of the synthetic ligand clozapine-N-oxide (CNO) (Figure S5A). Adult mice received the hM3Dq-EGFP retrovirus on the right DG and were studied 4 or 8 weeks later (Figures 5A and 5B). The day of in vivo stimulation, mice first received a CNO injection to activate hM3-GCs, then they were allowed to free exploration for 30 min to let basal activation of hippocampal networks, and brains were then collected 150 min after CNO administration for analysis of immediate-early gene expression by immunofluorescence. Analysis of Arc expression indicated that young and mature hM3-GCs displayed similar levels of activation by CNO in behaving mice (Figure 5C).

We then asked whether adult-born GCs recruit hilar parvalbumin[+] GABA interneurons (PV-INs), primary targets of mossy fibers and well known to be involved in perisomatic GABAergic inhibition of principal hippocampal cells (Freund and Buzsáki, 1996; Hosp et al., 2014; Kraushaar and Jonas, 2000). Activation of PV-INs was assessed by colocalization of PV with the immediate early gene c-Fos in the hilar region of both the ipsi- and contralateral hemispheres to the retroviral injection (Figure 5D). In the left hemisphere, contralateral to retroviral hM3Dq transduction, PV-INs displayed a baseline proportion of c-Fos expression of about 10%. Right hemispheres containing mature hM3-GCs displayed more than a 3-fold increase in the proportion of PV-INs expressing c-Fos, consistent with the recruitment of hilar GABAergic interneurons that support FBI (Figure 5E). In contrast, CNO-mediated activation of young hM3-GCs displayed only a slight nonsignificant change in PV-IN activation, in agreement with the poor recruitment of FBI described above. When comparing PV-IN activation among hemispheres ipsilateral to the retroviral transduction of EGFP (control) or hM3Dq, activation of mature hM3-GCs elicited a more than 2-fold increase in the proportion of PV-INs expressing c-Fos (Figure 5F). These experiments demonstrate that in vivo activation of mature but not young GCs activates hilar PV-INs, strengthening the differential recruitment of local hilar networks observed in slice recordings.

(D) (Left) Loose patch recordings in ChR2-GCs show similar reliability in laser (1 ms, blue line)-induced spiking in young and mature GCs. Scales, 50 pA (young), 200 pA (mature), 10 ms. (Right) Spiking reliability for young and mature ChR2-GCs (n = 7 young, n = 12 mature, p = 0.76).

(E) Example whole-cell voltage clamp recordings in a PC. (Left) Simplified scheme depicting light-activated pathways. (Right) Single laser pulses (1 ms, 0.07 Hz) delivered to young and mature ChR2-GCs elicit IPSCs (recorded at 0 mV, upper traces) and EPSCs (recorded at −70 mV, lower traces). Traces depict all sweeps in the experiment (gray) and their average (black). Scales, 50 pA, 20 ms (EPSCs), and 40 mV (IPSCs).

(F) Example voltage clamp recordings in mature (unlabeled) GCs. (Left) Simplified pathway scheme. (Right) Laser pulses elicited IPSCs, but not EPSCs (out of 60 recordings of young and mature ChR2-GCs, data not shown). Scale bars, 50 pA, 20 ms.

(G) Pharmacological blockade of light-evoked PSCs. Example subsequent traces show IPSC and EPSC blockade after bath application of NBQX (20 μM, red bar). Arrows denote the direction of temporal sequences. Scale bars, 100 pA, 40 ms (PC IPSCs), and 50 pA, 20 ms (PC EPSCs and GC IPSCs).

(H–J) Synaptic charge of laser-evoked responses. CA3 PC IPSC charge (H), p = 0.09, with n = 13 young and n = 15 mature. CA3 PC EPSC charge (I), p = 0.72, with n = 12 young and n = 13 mature. GC IPSC charge (J), p < 10^{-4}, with n = 26 young and n = 41 mature. All panels depict mean ± SEM. Hollow symbols correspond to the example traces. All statistical comparisons were performed using nonparametric two-tailed Mann-Whitney test. See also Figure S2.
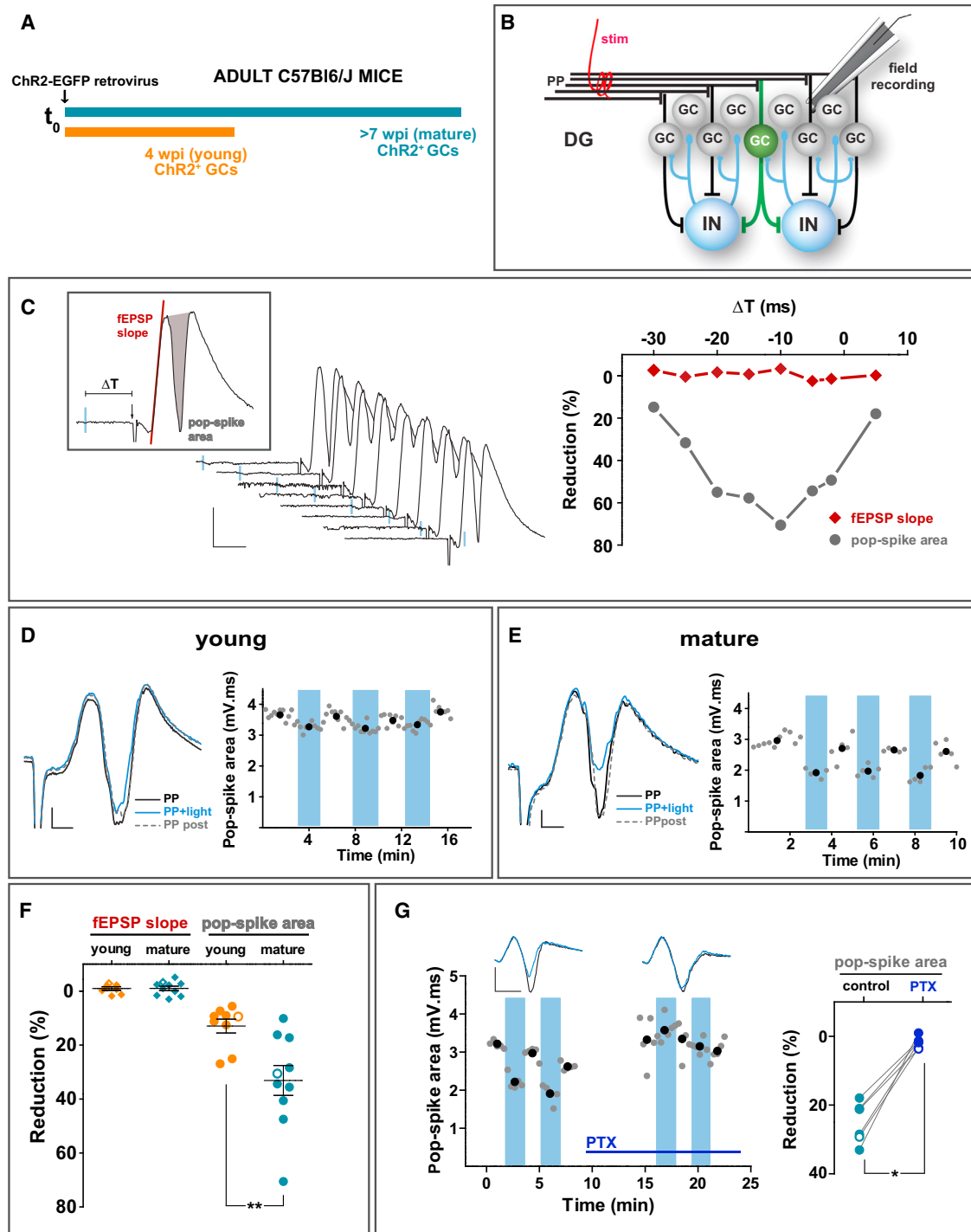
Figure 3. Mature GCs Control GCL Spiking by FBI

(A) Experimental design. A ChR2-EGFP retrovirus was injected in the adult DG and acute slices were obtained 4 (orange) or 7 (blue) weeks later.

(B) Simplified diagram of the recording configuration. A stimulation electrode (stim) was placed on the medial perforant path (mPP), and a field recording electrode was immersed into the GCL. Field responses were monitored after electrical stimulation alone or paired with light activation of ChR2-GCs to recruit FBI. IN, interneurons.

(C) (Left) Example experiment displaying field EPSP recordings for progressive delays (−30 to +5 ms) between the light pulse (blue line, 2 ms) and mPP stimulation (denoted by the downward deflection). Scales, 10 ms, 0.5 mV. The inset depicts parameters used to measure responses. (Right) Quantification of light-induced reduction of field responses defined as 100*(fEPSP$_{PP}$ − fEPSP$_{PP+light}$)/fEPSP$_{PP}$.

(legend continued on next page)

To determine whether PV-INs receive direct inputs from mature GCs, we performed retroviral ChR2 delivery in adult PV^{Cre};CAG^{FloxStopTom} mice (Hippenmeyer et al., 2005; Madisen et al., 2010) to render mature ChR2-GCs and tdTomato-labeled PV-INs (Tom-PV-INs; Figures 5G and 5H). Whole-cell recordings were performed in Tom-PV-INs to monitor synaptic responses evoked by activation of ChR2-GCs. Light stimulation induced fast and reliable EPSCs with a short delay to onset (about 5 ms; Figures 5I and 5J), consistent with a direct monosynaptic connection ChR2-GC → PV-IN. These experiments demonstrate that PV-INs are direct targets of adult-born mature GCs.

A Computational Model Predicts a Key Role for Delayed Coupling to Inhibition in the Discrimination of Novel Inputs

In line with the idea that new GCs learn to describe novel inputs not properly captured by previous experience (Aimone et al., 2011; Appleby and Wiskott, 2009; Wiskott et al., 2006), we propose a model where FBI differentiates the roles of young and mature GCs (Figure 6). We assume that the input space contains all possible patterns of activity in the neuronal layers that target the DG, among which the familiar ones are encoded by a large number of mature GCs through nonoverlapping input fields, due to the powerful FBI they recruit (Figures 6A and 6B, t_1). Young GCs, uncoupled from FBI, have large and overlapping input fields, which allow them to respond to novel inputs (Figures 6A and 6B, t_2). Maturation brings specialization as hebbian learning contributes to strengthen their association with some inputs, while progressive coupling to FBI reduces the size of input fields and their overlap (Figures 6A and 6B, t_3).

We performed computational simulations (see details in Supplemental Experimental Procedures and Figure S6), testing the acquisition of representations of a novel set of inputs by young GCs under three different scenarios: low inhibition, high inhibition, and transition from low to high inhibition, the latter mimicking the delayed coupling to inhibitory loops. In all cases, learning modified progressively the representation of the novel input space by the GC network until a steady state was reached (Figure 6D). However, it was only under the low-to-high inhibition condition that an ordered set of small and nonoverlapping input fields was acquired (Figure 6C), consistent with pattern separation (Figure 6E). These results suggest that delayed coupling to FBI could constitute an efficient network strategy with two concurring aims: (1) covering vast regions of potential inputs with a limited number of young GCs and (2) achieving a fine-grain representation of novel inputs.

DISCUSSION

Local Networks Activated by Adult-Born GCs

While mossy fiber targets have been characterized in depth, the way in which the feedback loops they activate impact onto the principal neuron layer (the GCL) has remained largely unexplored (Acsády et al., 1998; Freund and Buzsáki, 1996; Henze et al., 2002; Hosp et al., 2014; Jonas et al., 1993; Kraushaar and Jonas, 2000; Torborg et al., 2010). Using optogenetics and synthetic G-coupled receptors to stimulate specific neuronal populations allowed us to dissect the postsynaptic pathways recruited by GCs. We show that mature GCs activate the canonical DG outputs that include the mossy fiber–CA3 pyramidal cell synapse, the mossy fiber–GABA interneuron–CA3 pyramidal cell feedforward pathway, and the mossy fiber–GABA interneuron–GC feedback loop, regardless of whether GCs were generated during early postnatal or adult neurogenesis. We also demonstrate that the synchronous activation of a small number of mature GCs (tens of neurons) may recruit powerful FBI that can substantially reduce the gain of the GCL and thus decrease the proportion of active GCs. These findings provide experimental evidence for the contribution of FBI to sparse coding in the GCL, a hallmark in DG processing (Chawla et al., 2005; Leutgeb et al., 2007; Neunuebel and Knierim, 2014; Treves et al., 2008).

We found no conclusive evidence to support an excitatory feedback loop onto the GCL. Given that hilar mossy cells receive synaptic inputs from GCs and target their proximal dendrites, the lack of excitatory currents reflecting the GC–mossy cell–GC loop may be a consequence of the septotemporal organization of mossy cell projections, severed in our transverse slice preparation (Amaral and Witter, 1989). However, since mossy cells also target GABAergic interneurons, it is possible that they contribute to the FBI component observed here (Jinde et al., 2012; Scharfman, 1995).

The dentate network contains distinct types of GABAergic interneurons with diverse morphofunctional characteristics that could mediate FBI, including PV-expressing basket and axoaxonic cells that target GCs (Freund and Buzsáki, 1996; Hosp et al., 2014). Our in vitro and in vivo data show that immature GCs poorly recruit PV-INs and FBI loops, while mature GCs can activate both PV-INs and FBI. We also show that adult-born GCs establish strong synaptic connections onto PV-INs, with sufficient strength for spike generation (Figures 5 and S5B). These findings suggest that PV-INs may be an important component of the FBI loop that, together with the FFI, controls how the principal layer responds to incoming inputs. In our experiments, the magnitude of FBI recruited by mature GCs appears much smaller

---

(D and E) Representative experiments for young (D) and mature (E) ChR2-GCs depicting fEPSPs recorded in response to low frequency stimulation (0.07 Hz) of mPP alone (PP), paired with a preceding light pulse (−10 ms, 2 ms duration; PP + light), and subsequent PP alone (PP post). Scale bars, 2 ms, 0.2 mV. In the quantitative plots, blue columns denote trials where mPP stimulation is paired with light. Black dots are average values taken within the colored or white columns.
(F) Optogenetic preactivation (−10 ms) of ChR2-GCs reduces spiking of the GC layer. Quantification of responses (mean ± SEM) is the same as in (C). Light pulses elicited no changes in fEPSP slope (young, p = 0.16; mature, p = 0.27; Wilcoxon signed rank test). Pop spikes were reduced in both groups by optogenetic pairing, with a significantly larger pop-spike reduction for mature versus young ChR2-GCs. Data were obtained from 9 slices/5 mice (young) and 10 slices/5 mice (mature). **p < 0.01, two-tailed Mann-Whitney's test.
(G) Pharmacological blockade of FBI recruited by mature GCs. (Left) Representative experiment similar to the one shown in (E), before and after bath application of PTX (100 μM, horizontal bar). Scale bars, 5 ms, 0.5 mV. (Right) Reduction of pop spike by stimulation of mature ChR2-GCs before (control) and after PTX. Data were obtained from 6 slices/4 mice. *p < 0.05 Wilcoxon matched pairs signed rank test. Hollow symbols in (F) and (G) correspond to the example traces. See also Figure S3.
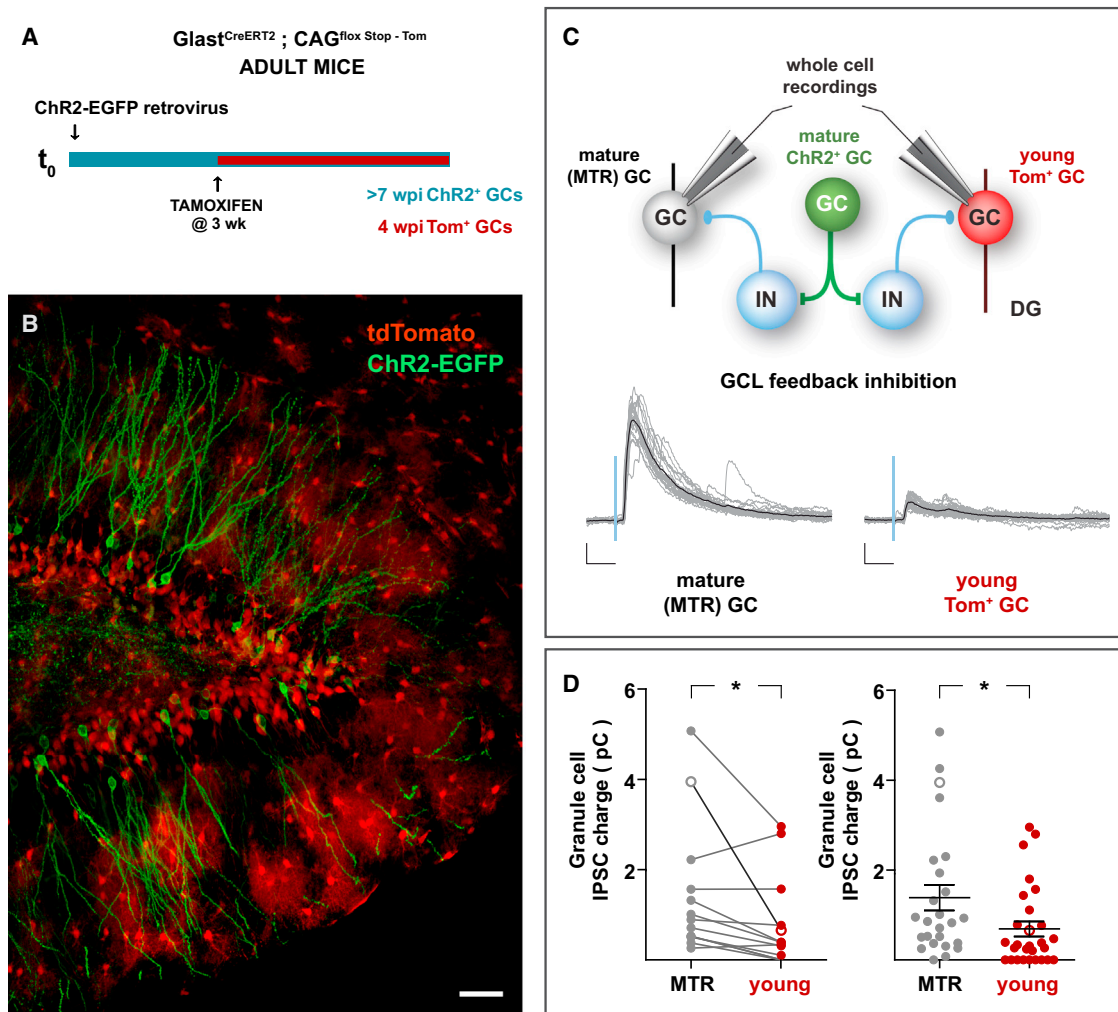
Figure 4. Immature GCs Receive Weak FBI

(A and B) Experimental design. Young adult GLAST^{CreERT2};CAG^{floxStopTom} mice received a ChR2-EGFP retrovirus in the right DG, followed by administration of TAM 3–4 weeks later. Mice were sacrificed 4 weeks later, rendering mature GCs expressing ChR2-EGFP, and young cells expressing Tom, as shown in the confocal image (B). Tom$^+$ astrocytes are also observed, particularly in the molecular layer. Scale bar, 50 μm.

(C) (Top) Simplified network schematic depicting the recording conditions. Light stimulation of mature ChR2-GCs activate local networks, and whole-cell recordings are obtained from young (Tom$^+$) or mature (unlabeled) GCs to compare the amount of FBI they receive. (Bottom) Example recordings depicting light-evoked FBI onto mature (MTR) and young (Tom) GCs. Traces depict all IPSC sweeps in the experiment (gray) and their average (black). Scales, 50 pA, 20 ms.

(D) Synaptic charge of laser-evoked responses. (Left) Paired analysis of IPSCs evoked onto young and mature GCs recorded within the same optic field. *p < 0.02, with n = 13, two-tailed Wilcoxon matched pairs signed rank test. (Right) Analysis of all light-evoked IPSC. *p < 0.02, with n = 25 mature (MTR) and n = 28 young (Tom), two-tailed Mann-Whitney's test (data shown as mean ± SEM). In both panels, hollow symbols indicate the examples shown in (C). See also Figure S4.

than the FFI activated by PP stimulation (Figure S3). This observation most likely reflects the combination of an electrical stimulus that recruits thousands of axons in the PP with a light pulse that recruits tens of ChR2-GCs present in the slice. Notably, in spite of this difference, FBI can strongly change the excitation/inhibition balance and influence spiking in the GCL when this inhibition occurs within the phase of membrane depolarization.

A New Component in the Critical Period of Developing Adult-Born GCs

We aimed to understand how adult-born GCs influence the local networks where they integrate, and at what develop-

mental stages they may begin to modify the input/output properties in the dentate. This information would contribute to better understanding the benefit of adult neurogenesis for hippocampal function (Drew et al., 2013; Marín-Burgin et al., 2012; Neunuebel and Knierim, 2012; Piatti et al., 2013). We focused on young GCs undergoing a critical period that was previously defined in regard to their high activity rate, enhanced synaptic plasticity, reduced responsiveness to FFI, and poor input specificity (Dieni et al., 2013; Espósito et al., 2005; Ge et al., 2007; Gu et al., 2012; Marín-Burgin et al., 2012; Mongiat et al., 2009; Schmidt-Hieber et al., 2004; Snyder et al., 2001). The data presented here reveal a new characteristic of this critical
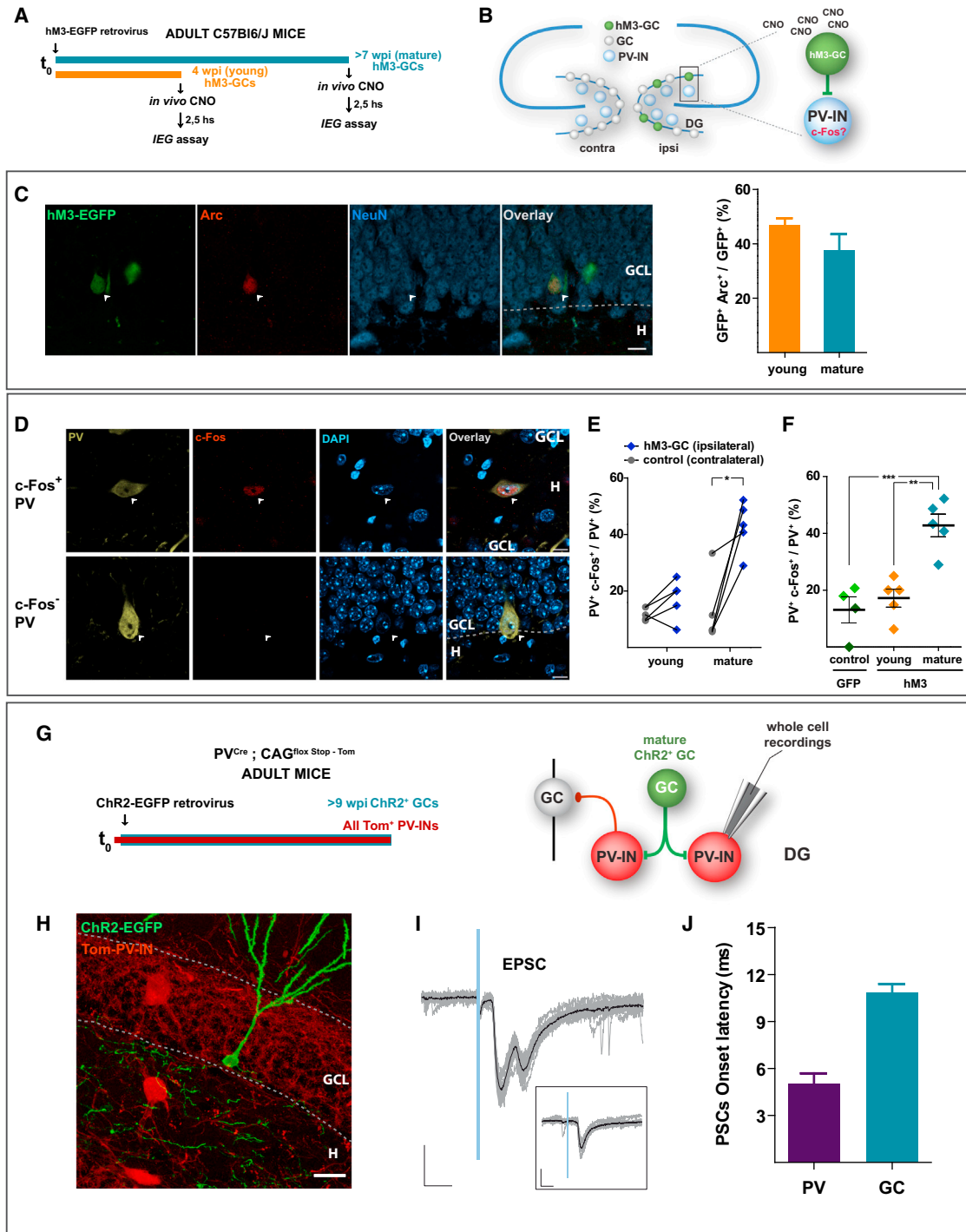
Figure 5. In Vivo Activation of PV Interneurons by Mature Adult-Born GCs

(A) Experimental design. Adult mice received a retrovirus expressing the hM3-EGFP synthetic receptor in the right dentate gyrus. Four or 8 weeks later, mice received the synthetic agonist CNO (5 μg/g, i.p.), were allowed to free exploration for 30 min, and were sacrificed 150 min after CNO administration. Immediate-early genes (IEGs) were detected by immunofluorescence.

(B) Rationale: the right DG (ipsilateral) contains young or mature hM3-GCs. CNO will reach the whole brain, but will only activate hM3-GCs in the right DG. Activation of PV+ hilar interneurons (PV-INs) is assessed by c-Fos expression in both hemispheres.

(C) Activation of hM3-GCs by CNO. (Left) Single-plane confocal image of ipsilateral DG showing mature hM3-EGFP+ GCs (green), Arc expression (red), NeuN (blue), and the overlay. Calibration bar, 10 μm. The granule cell layer (GCL) and hilar areas (H) are separated by the dotted line. (Right) Quantification of the proportion of young and mature hM3-GCs expressing Arc. n = 5 mice (for both each group), p = 0.20, two-tailed t test.

(legend continued on next page)

period, the reduced recruitment of FBI networks by mossy fibers.

Immature GCs present a remarkable delay in the recruitment of proximal targets, since their mossy fiber projections onto the more distal CA3 targets are highly functional. The duration of this immature stage might also be prone to modulation by network activity and cognitive demand (Piatti et al., 2011; Tronel et al., 2010). As they mature, GCs decrease their excitability, become tightly coupled to inhibitory circuits, and reduce their ability to refine glutamatergic connections. Our data demonstrate that once the critical period has finished, mature adult-born GCs recruit inhibitory feedback loops that influence the activity of the dentate input layer, the GCL. We speculate that the transition from poor to strong coupling to local GABAergic networks does in fact contribute to define the critical period; increasing inhibition would reduce GCs activation and would also generate more stringent conditions for activity-dependent synaptic plasticity of excitatory connections (Dan and Poo, 2004; Marín-Burgin et al., 2012; Pouille and Scanziani, 2001). In this context, the critical period described for adult-born GCs would not be a mere transition toward a final state of functional integration but, rather, a necessary mechanism for information processing in the hippocampus.

EXPERIMENTAL PROCEDURES

Animals and Surgery for Retroviral Delivery

Male C57Bl/6J mice 5–7 weeks of age were housed at two to four mice per cage. Running wheel housing started 2–4 days before surgery and continued until the day of slice preparation, to maximize the number of retrovirally transduced neurons. For surgery, mice were anesthetized (150 μg ketamine/15 μg xylazine in 10 μl saline/g), and virus (1–1.5 μl at 0.15 μl/min) was infused into the dorsal area of the right dentate gyrus using sterile microcapillary calibrated pipettes (Drummond Scientific, Broomall, PA) and stereotaxic references (coordinates from bregma, −2 mm anteroposterior, −1.5 mm lateral, −1.9 mm ventral). Animals were killed for acute slice preparation at the indicated times. Experimental protocols were approved by the Institutional Animal Care and Use Committee of the Leloir Institute according to the Principles for Biomedical Research involving animals of the Council for International Organizations for Medical Sciences and provisions stated in the Guide for the Care and Use of Laboratory Animals. Genetically modified mice were utilized when the retroviral approach was suboptimal or in experiments that required identifying multiple neuronal populations (see Supplemental Experimental Procedures).

Retroviral Vectors

A replication-deficient retroviral vector based on the Moloney murine leukemia virus was used to specifically transduce adult-born GCs as done previously (Marín-Burgin et al., 2012; Piatti et al., 2011). Retroviral particles were assembled using three separate plasmids containing the capside (CMV-vsvg), viral proteins (CMV-gag/pol), and the transgenes: CAG-GFP, channelrhodopsin-2 (ChR2; Ubi-ChR2-EGFP retroviral plasmid, kindly provided by S. Ge, SUNY Stony Brook), or the synthetic G-coupled receptor hM3Dq (CAG-EGFP-2A-hM3Dq) (Alexander et al., 2009). hM3Dq was kindly provided by B. Roth (University of North Carolina at Chapel Hill). Plasmids were transfected onto HEK293T cells using deacylated polyethylenimine. Virus-containing supernatant was harvested 48 hr after transfection and concentrated by two rounds of ultracentrifugation. Virus titer was typically ∼10^5 particles/μl.

Electrophysiological Recordings
Slice Preparation

Mice were anesthetized and decapitated at 4 or 7–8 weeks postinjection (wpi) as indicated, and transverse slices were prepared as described previously (Marín-Burgin et al., 2012) (see also Supplemental Experimental Procedures).

Electrophysiology

Recorded neurons were visually identified by fluorescence and infrared DIC videomicroscopy. Whole-cell recordings were performed using microelectrodes (3–5 MΩ) filled with (in mM) 130 CsOH, 130 D-gluconic acid, 3 MgCl2, 0.2 EGTA, 1 NaCl, 0.4 CsCl, 10 HEPES, 4 ATP-tris, 0.3 GTP-tris, and 10 phosphocreatine. Loose-patch recordings were performed with ACSF-filled patch pipettes (8–10 MΩ). Field recordings were performed using patch pipettes (2–4 MΩ) filled with 3M NaCl. All recordings were obtained using Axopatch 200B amplifiers (Molecular Devices, Sunnyvale, CA), digitized (Digidata 1322A, Molecular Devices), and acquired at 10 KHz onto a personal computer using the pClamp 9 software (Molecular Devices).

Optogenetics

Hippocampal slices containing GCs expressing ChR2 (ChR2-GCs) were prepared 4 or 7–8 weeks after retroviral delivery, or 9 weeks after Tam-induced recombination (for Ascl1^{CreERT2};CAG^{floxStopChR2} mice). ChR2-GCs were stimulated using a 447 nm laser source delivered through the epifluorescence pathway of the upright microscope (FITC filter, 63× objective for whole-cell recordings, 20× for field recordings) commanded by the acquisition software. See additional details in Supplemental Experimental Procedures.

Field Recordings

Medial perforant path (mPP) stimulation was performed by placing a steel monopolar electrode in the middle of the molecular layer, and current pulses ranging from 35 to 200 μA (100 μs) were applied at 0.07 Hz. The recording microelectrode was placed in the GCL to record the population spike (pop spike) in response to mPP stimulation (Marín-Burgin et al., 2012). Experiments were performed at stimulus intensities that evoked 25%–50% of maximal pop-spike amplitude. Population activity was recorded by several subsequent trials until stable pop-spike amplitude was obtained. At that moment, a laser pulse (2 ms) was paired to mPP stimulation at different times (as indicated): −10 ms for most experiments. At least 25 trials were recorded to evaluate the effect of optogenetically activated FBI on the GCL pop spike.

FBI onto Immature GCs

See Supplemental Experimental Procedures.

(D) Activation of PV-INs assessed by c-fos immunofluorescence. Single-plane confocal images showing a c-Fos⁺ (red) and a c-Fos⁻ PV-IN (bronze) in a DAPI (blue) background. Scale, 20 μm.

(E and F) Quantitative analysis of PV-INs activation by hM3-GCs. (E) Paired comparison of PV-IN activation in the ipsi- versus contralateral DGs for young and mature hM3-GCs. Each pair of dots correspond to one mouse (n = 231 PV-INs, 5 mice [young GCs]; and n = 296 PV-INs, 5 mice [mature GCs]). *p < 0.02, two-tailed paired t test. (F) Comparison of activation of PV interneurons in the ipsilateral DG of EGFP-GCs (control, n = 2 mice at 4 wpi [light green]; and n = 2 mice at 8 wpi [dark green], 108 PV-INs), young hM3-GCs, and mature hM3-GCs. **p < 0.01 and ***p < 0.001 after one-way ANOVA (p < 0.001) and post hoc Bonferroni's test.

(G–J) Electrophysiological recordings of ChR2-GC → PV-IN synaptic connections in acute slices. (G) Adult PV^{Cre};CAG^{floxStopTom} mice received a ChR2-EGFP retrovirus in the right DG and were sacrificed >9 weeks later, rendering mature GCs expressing ChR2-EGFP, and PV-INs expressing Tom (Tom-PV-INs). (H) Confocal image depicting ChR2-GCs (EGFP) and Tom-PV-INs in a slice used for electrophysiological recordings. Scale bar, 20 μm. (I) Example whole-cell recording of Tom-PV-INs displaying EPSCs elicited by light stimulation of mature ChR2-GCs (n = 8 Tom-PV-INs). Note that the second peak in the current traces seems to arise from a polysynaptic connection, and it disappears when laser power is reduced to 25% (inset). Traces depict all sweeps in the experiment (gray) and their average (black). Scales, 50 pA, 10 ms. (J) Fast latency to onset of ChR2 EPSC onto Tom-PV-INs (n = 8 Tom-PV-INs), consistent with a monosynaptic connection. Compare with the prolonged delay of feedback IPSCs recorded in mature GCs (n = 40 GCs, same data as shown in Figure S2A). Data are depicted as mean ± SEM. See also Figure S5.
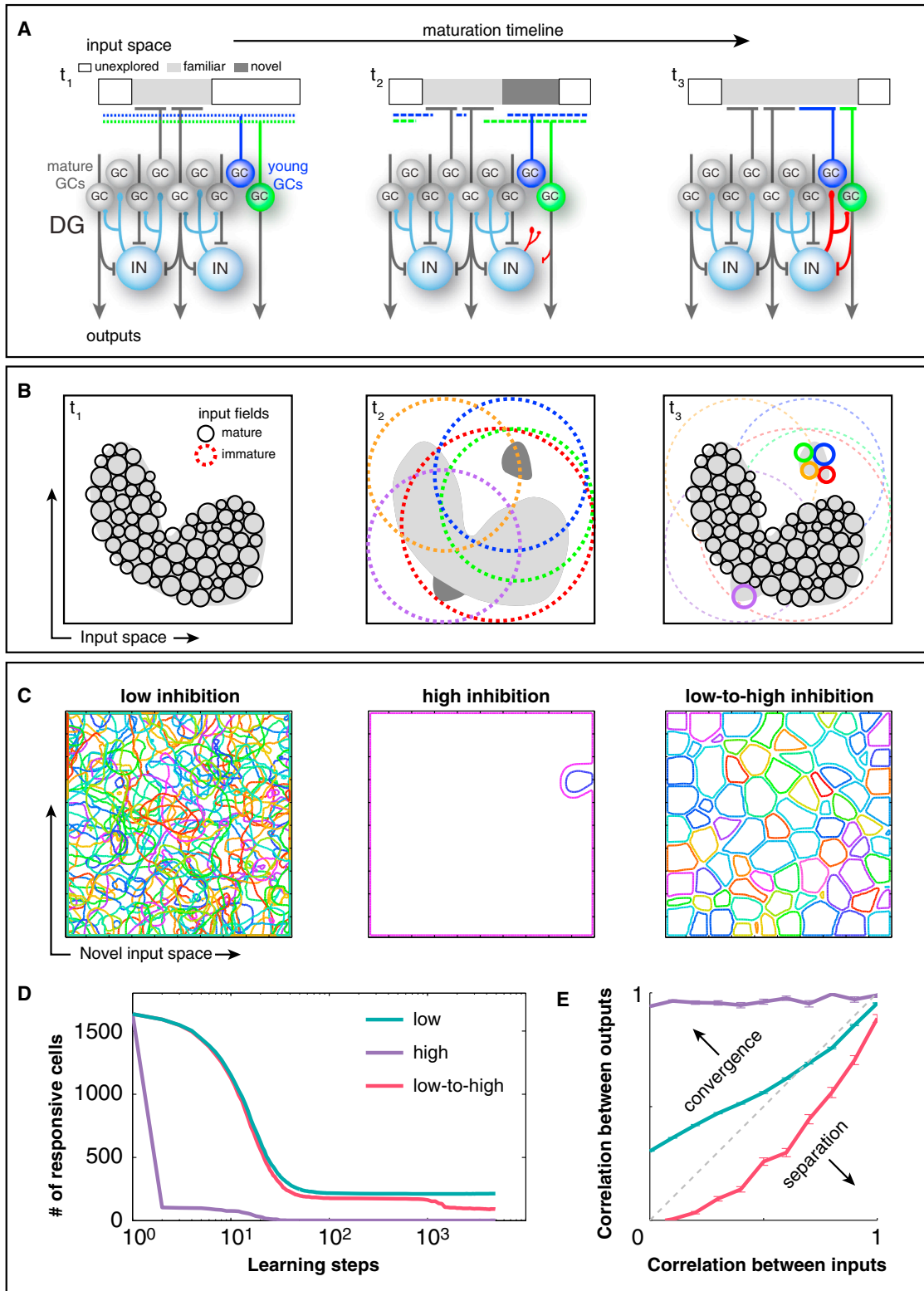
Figure 6. The Delayed Coupling of Young GCs to FBI Networks Could Be Crucial to Achieve a Fine-Grain Representation of Novel Inputs, as Revealed by Computational Simulations

(A) The ensemble of all possible input patterns to the dentate gyrus is divided into familiar (light gray), novel (dark gray), and unexplored (white), the latter accounting for most of the input space. Three snapshots of the maturation timeline are represented. The input of a developing GC is tuned toward novelty through

(legend continued on next page)

Data Analysis

Analysis of whole-cell and field recordings was performed offline using in-house-made Matlab routines. In all cases reported PSCs values for charge and peak amplitude correspond to the product of the mean value for positive trials and the probability of success, taken as the fraction of trials in which an evoked response was observed.

Statistical Analysis

Unless otherwise specified, data are presented as mean ± SEM. Normality was assessed using Shapiro-Wilk's test, D'Agostino & Pearson omnibus test, and Kolmogórov-Smirnov's test, at a p value of 0.05. A distribution was considered as normal if all tests were passed. When a data set did not satisfy normality criteria, nonparametric statistics were applied. Two-tailed Mann-Whitney's test was used for single comparisons, and two-tailed Wilcoxon matched pairs signed rank test was used for paired values. For normal distributions, homoscedasticity was assessed using Bartlett's test and F-test, at a p value of 0.05. For homogeneous variances, two-tailed t test was used for single comparisons, and one-way ANOVA followed by post hoc Bonferroni's test was used for multiple comparisons. Paired t test was used to compare paired data. In the only case were variances were not homogeneous, a t test with Welch's correction was used.

Further details about immunofluorescence, confocal microscopy, and in vivo assays are provided in the Supplemental Experimental Procedures.

SUPPLEMENTAL INFORMATION

Supplemental Information includes seven figures and Supplemental Experimental Procedures and can be found with this article at http://dx.doi.org/10.1016/j.neuron.2014.11.023.

AUTHOR CONTRIBUTIONS

S.G.T., L.A.M., and S.M.Y. are the leading authors, contributed to the concept, designed and performed the experiments, analyzed the data, and edited the manuscript. M.F.T. performed in vivo experiments and analyzed the data. D.D.A. characterized the Ascl1[CreERT2] mice and the HM3Dq-expressing cells, performed immunofluorescence and confocal imaging, and analyzed the data. E.K. elaborated the computational model. D.G. assembled the HM3Dq retrovirus and contributed to the initial HM3Dq characterization. N.B. prepared all retroviruses. G.M.L. provided expertise on the use of genetically modified mice and contributed with insightful ideas. A.F.S. contributed to the concept, designed the experiments, analyzed the data, wrote the manuscript, and provided financial support.

REFERENCES

Acsády, L., Kamondi, A., Sík, A., Freund, T., and Buzsáki, G. (1998). GABAergic cells are the major postsynaptic targets of mossy fibers in the rat hippocampus. J. Neurosci. 18, 3386–3403.

Aimone, J.B., Deng, W., and Gage, F.H. (2011). Resolving new memories: a critical look at the dentate gyrus, adult neurogenesis, and pattern separation. Neuron 70, 589–596.

Alexander, G.M., Rogan, S.C., Abbas, A.I., Armbruster, B.N., Pei, Y., Allen, J.A., Nonneman, R.J., Hartmann, J., Moy, S.S., Nicolelis, M.A., et al. (2009). Remote control of neuronal activity in transgenic mice expressing evolved G protein-coupled receptors. Neuron 63, 27–39.

Altman, J., and Bayer, S.A. (1990). Migration and distribution of two populations of hippocampal granule cell precursors during the perinatal and postnatal periods. J. Comp. Neurol. 301, 365–381.

Amaral, D.G., and Witter, M.P. (1989). The three-dimensional organization of the hippocampal formation: a review of anatomical data. Neuroscience 31, 571–591.

Andersen, P., Morris, R.G., Amaral, D.G., Bliss, T.V., and O'Keefe, J. (2007). Historical perspective: proposed funcitons, biological characteristics, and neurobiological models of the hippocampus. In The Hippocampus Book, P. Andersen, R.G. Morris, D.G. Amaral, T.V. Bliss, and J. O'Keefe, eds. (New York: Oxford University Press), pp. 9–36.

Appleby, P.A., and Wiskott, L. (2009). Additive neurogenesis as a strategy for avoiding interference in a sparsely-coding dentate gyrus. Network 20, 137–161.

the concurrence of hyperexcitability, enhanced hebbian learning, and the gradual incorporation of inhibitory feedback from and to the GC population (red connections). Its input field at t_1 is broad and unspecific, but competition with mature cells gradually banishes it from all well-represented input regions. Hebbian learning reinforces its tuning to available niches of poorly represented inputs, such as the novel input introduced at t_2. By the end of the learning process (t_3), it has developed a specific response to those novel inputs that, in turn, become familiar.

(B) Representation of the same input space from the perspective of population coding. Each circle denotes the input field of a GC. The representation of the familiar input space by the mature GC population is characterized by high specialization: input fields are small and tightly packed, presenting low levels of overlap that are supported by FBI. Hence, similar inputs are likely to be represented by different GCs. Immature GCs, instead, lack FBI and therefore display overlapping input fields, as represented at t_2. This condition allows them to cover not only the familiar input space but also unexplored input regions, which ensures that many of them will respond to novel inputs, such as the ones introduced at t_2. Hebbian learning and FBI progressively transform their broad and overlapping input fields into small and nonoverlapping, until they gain at t_3 a mature level of specialization. Novel inputs are now encoded with a fine-grain scale that promotes separation.

(C) A computational model (Figure S6) shows that such a fine-grain representation of novel inputs can only be achieved when young GCs are slowly introduced into the FBI circuit (low-to-high inhibition protocol). On the contrary, if young GCs are subject to fixed levels of inhibition, they develop wide fields with low discrimination power, both for low levels of FBI (many cells with overlapping fields) and high levels of FBI (few cells with nonoverlapping fields).

(D) Variation of the number of responsive neurons (activity higher than 0.5 for some region of the input space) along the training process. Note that in all cases it takes many iterations for the network to evolve to a stable state. This shows that the different behaviors are not a mere consequence of initial conditions, but rather that the dynamics of learning under different inhibition protocols exerts a strong influence on the final state of the network.

(E) Correlations of pairs of population activity vectors at the input (EC) and output (DG) layers were compared (mean ± SEM). Only the low-to-high inhibition protocol generates representations in the GC layer that are more dissimilar than the corresponding inputs (pattern separation). Curves follow the same color code as in (D). For details on the model, see also Figure S6.

Caroni, P., Donato, F., and Muller, D. (2012). Structural plasticity upon learning: regulation and functions. Nat. Rev. Neurosci. *13*, 478–490.

Chancey, J.H., Adlaf, E.W., Sapp, M.C., Pugh, P.C., Wadiche, J.I., and Overstreet-Wadiche, L.S. (2013). GABA depolarization is required for experience-dependent synapse unsilencing in adult-born neurons. J. Neurosci. *33*, 6614–6622.

Chawla, M.K., Guzowski, J.F., Ramirez-Amaya, V., Lipa, P., Hoffman, K.L., Marriott, L.K., Worley, P.F., McNaughton, B.L., and Barnes, C.A. (2005). Sparse, environmentally selective expression of Arc RNA in the upper blade of the rodent fascia dentata by brief spatial experience. Hippocampus *15*, 579–586.

Chiang, P.H., Wu, P.Y., Kuo, T.W., Liu, Y.C., Chan, C.F., Chien, T.C., Cheng, J.K., Huang, Y.Y., Chiu, C.D., and Lien, C.C. (2012). GABA is depolarizing in hippocampal dentate granule cells of the adolescent and adult rats. J. Neurosci. *32*, 62–67.

Clelland, C.D., Choi, M., Romberg, C., Clemenson, G.D., Jr., Fragniere, A., Tyers, P., Jessberger, S., Saksida, L.M., Barker, R.A., Gage, F.H., and Bussey, T.J. (2009). A functional role for adult hippocampal neurogenesis in spatial pattern separation. Science *325*, 210–213.

Creer, D.J., Romberg, C., Saksida, L.M., van Praag, H., and Bussey, T.J. (2010). Running enhances spatial pattern separation in mice. Proc. Natl. Acad. Sci. USA *107*, 2367–2372.

Dan, Y., and Poo, M.M. (2004). Spike timing-dependent plasticity of neural circuits. Neuron *44*, 23–30.

Deshpande, A., Bergami, M., Ghanem, A., Conzelmann, K.K., Lepier, A., Götz, M., and Berninger, B. (2013). Retrograde monosynaptic tracing reveals the temporal evolution of inputs onto new neurons in the adult dentate gyrus and olfactory bulb. Proc. Natl. Acad. Sci. USA *110*, E1152–E1161.

Dieni, C.V., Nietz, A.K., Panichi, R., Wadiche, J.I., and Overstreet-Wadiche, L. (2013). Distinct determinants of sparse activation during granule cell maturation. J. Neurosci. *33*, 19131–19142.

Drew, L.J., Fusi, S., and Hen, R. (2013). Adult neurogenesis in the mammalian hippocampus: why the dentate gyrus? Learn. Mem. *20*, 710–729.

Dupret, D., Revest, J.M., Koehl, M., Ichas, F., De Giorgi, F., Costet, P., Abrous, D.N., and Piazza, P.V. (2008). Spatial relational memory requires hippocampal adult neurogenesis. PLoS ONE *3*, e1959.

Espósito, M.S., Piatti, V.C., Laplagne, D.A., Morgenstern, N.A., Ferrari, C.C., Pitossi, F.J., and Schinder, A.F. (2005). Neuronal differentiation in the adult hippocampus recapitulates embryonic development. J. Neurosci. *25*, 10074–10086.

Faulkner, R.L., Jang, M.H., Liu, X.B., Duan, X., Sailor, K.A., Kim, J.Y., Ge, S., Jones, E.G., Ming, G.L., Song, H., and Cheng, H.J. (2008). Development of hippocampal mossy fiber synaptic outputs by new neurons in the adult brain. Proc. Natl. Acad. Sci. USA *105*, 14157–14162.

Freund, T.F., and Buzsáki, G. (1996). Interneurons of the hippocampus. Hippocampus *6*, 347–470.

Ge, S., Goh, E.L., Sailor, K.A., Kitabatake, Y., Ming, G.L., and Song, H. (2006). GABA regulates synaptic integration of newly generated neurons in the adult brain. Nature *439*, 589–593.

Ge, S., Yang, C.H., Hsu, K.S., Ming, G.L., and Song, H. (2007). A critical period for enhanced synaptic plasticity in newly generated neurons of the adult brain. Neuron *54*, 559–566.

Gu, Y., Arruda-Carvalho, M., Wang, J., Janoschka, S.R., Josselyn, S.A., Frankland, P.W., and Ge, S. (2012). Optical controlling reveals time-dependent roles for adult-born dentate granule cells. Nat. Neurosci. *15*, 1700–1706.

Henze, D.A., Wittner, L., and Buzsáki, G. (2002). Single granule cells reliably discharge targets in the hippocampal CA3 network in vivo. Nat. Neurosci. *5*, 790–795.

Hippenmeyer, S., Vrieseling, E., Sigrist, M., Portmann, T., Laengle, C., Ladle, D.R., and Arber, S. (2005). A developmental switch in the response of DRG neurons to ETS transcription factor signaling. PLoS Biol. *3*, e159.

Holtmaat, A., and Svoboda, K. (2009). Experience-dependent structural synaptic plasticity in the mammalian brain. Nat. Rev. Neurosci. *10*, 647–658.

Hosp, J.A., Strüber, M., Yanagawa, Y., Obata, K., Vida, I., Jonas, P., and Bartos, M. (2014). Morpho-physiological criteria divide dentate gyrus interneurons into classes. Hippocampus *24*, 189–203.

Jinde, S., Zsiros, V., Jiang, Z., Nakao, K., Pickel, J., Kohno, K., Belforte, J.E., and Nakazawa, K. (2012). Hilar mossy cell degeneration causes transient dentate granule cell hyperexcitability and impaired pattern separation. Neuron *76*, 1189–1200.

Jonas, P., Major, G., and Sakmann, B. (1993). Quantal components of unitary EPSCs at the mossy fibre synapse on CA3 pyramidal cells of rat hippocampus. J. Physiol. *472*, 615–663.

Kim, E.J., Leung, C.T., Reed, R.R., and Johnson, J.E. (2007). In vivo analysis of Ascl1 defined progenitors reveals distinct developmental dynamics during adult neurogenesis and gliogenesis. J. Neurosci. *27*, 12764–12774.

Kraushaar, U., and Jonas, P. (2000). Efficacy and stability of quantal GABA release at a hippocampal interneuron-principal neuron synapse. J. Neurosci. *20*, 5594–5607.

Laplagne, D.A., Espósito, M.S., Piatti, V.C., Morgenstern, N.A., Zhao, C., van Praag, H., Gage, F.H., and Schinder, A.F. (2006). Functional convergence of neurons generated in the developing and adult hippocampus. PLoS Biol. *4*, e409.

Leutgeb, J.K., Leutgeb, S., Moser, M.B., and Moser, E.I. (2007). Pattern separation in the dentate gyrus and CA3 of the hippocampus. Science *315*, 961–966.

Li, Y., Stam, F.J., Aimone, J.B., Goulding, M., Callaway, E.M., and Gage, F.H. (2013). Molecular layer perforant path-associated cells contribute to feed-forward inhibition in the adult dentate gyrus. Proc. Natl. Acad. Sci. USA *110*, 9106–9111.

Madisen, L., Zwingman, T.A., Sunkin, S.M., Oh, S.W., Zariwala, H.A., Gu, H., Ng, L.L., Palmiter, R.D., Hawrylycz, M.J., Jones, A.R., et al. (2010). A robust and high-throughput Cre reporting and characterization system for the whole mouse brain. Nat. Neurosci. *13*, 133–140.

Madisen, L., Mao, T., Koch, H., Zhuo, J.M., Berenyi, A., Fujisawa, S., Hsu, Y.W., Garcia, A.J., 3rd, Gu, X., Zanella, S., et al. (2012). A toolbox of Cre-dependent optogenetic transgenic mice for light-induced activation and silencing. Nat. Neurosci. *15*, 793–802.

Marín-Burgin, A., Mongiat, L.A., Pardi, M.B., and Schinder, A.F. (2012). Unique processing during a period of high excitation/inhibition balance in adult-born neurons. Science *335*, 1238–1242.

Markwardt, S.J., Wadiche, J.I., and Overstreet-Wadiche, L.S. (2009). Input-specific GABAergic signaling to newborn neurons in adult dentate gyrus. J. Neurosci. *29*, 15063–15072.

Markwardt, S.J., Dieni, C.V., Wadiche, J.I., and Overstreet-Wadiche, L. (2011). Ivy/neurogliaform interneurons coordinate activity in the neurogenic niche. Nat. Neurosci. *14*, 1407–1409.

Mathews, E.A., Morgenstern, N.A., Piatti, V.C., Zhao, C., Jessberger, S., Schinder, A.F., and Gage, F.H. (2010). A distinctive layering pattern of mouse dentate granule cells is generated by developmental and adult neurogenesis. J. Comp. Neurol. *518*, 4479–4490.

Ming, G.L., and Song, H. (2011). Adult neurogenesis in the mammalian brain: significant answers and significant questions. Neuron *70*, 687–702.

Mongiat, L.A., and Schinder, A.F. (2011). Adult neurogenesis and the plasticity of the dentate gyrus network. Eur. J. Neurosci. *33*, 1055–1061.

Mongiat, L.A., Espósito, M.S., Lombardi, G., and Schinder, A.F. (2009). Reliable activation of immature neurons in the adult hippocampus. PLoS ONE *4*, e5320.

Mori, T., Tanaka, K., Buffo, A., Wurst, W., Kühn, R., and Götz, M. (2006). Inducible gene deletion in astroglia and radial glia—a valuable tool for functional and lineage analysis. Glia *54*, 21–34.

Nakashiba, T., Cushman, J.D., Pelkey, K.A., Renaudineau, S., Buhl, D.L., McHugh, T.J., Rodriguez Barrera, V., Chittajallu, R., Iwamoto, K.S., McBain, C.J., et al. (2012). Young dentate granule cells mediate pattern separation, whereas old granule cells facilitate pattern completion. Cell *149*, 188–201.

Neunuebel, J.P., and Knierim, J.J. (2012). Spatial firing correlates of physiologically distinct cell types of the rat dentate gyrus. J. Neurosci. *32*, 3848–3858.

Neunuebel, J.P., and Knierim, J.J. (2014). CA3 retrieves coherent representations from degraded input: direct evidence for CA3 pattern completion and dentate gyrus pattern separation. Neuron *81*, 416–427.

Overstreet-Wadiche, L.S., Bensen, A.L., and Westbrook, G.L. (2006). Delayed development of adult-generated granule cells in dentate gyrus. J. Neurosci. *26*, 2326–2334.

Piatti, V.C., Davies-Sala, M.G., Espósito, M.S., Mongiat, L.A., Trinchero, M.F., and Schinder, A.F. (2011). The timing for neuronal maturation in the adult hippocampus is modulated by local network activity. J. Neurosci. *31*, 7715–7728.

Piatti, V.C., Ewell, L.A., and Leutgeb, J.K. (2013). Neurogenesis in the dentate gyrus: carrying the message or dictating the tone. Front. Neurosci. *7*, 50.

Pouille, F., and Scanziani, M. (2001). Enforcement of temporal fidelity in pyramidal cells by somatic feed-forward inhibition. Science *293*, 1159–1163.

Ramirez-Amaya, V., Marrone, D.F., Gage, F.H., Worley, P.F., and Barnes, C.A. (2006). Integration of new neurons into functional neural networks. J. Neurosci. *26*, 12237–12241.

Sahay, A., Scobie, K.N., Hill, A.S., O'Carroll, C.M., Kheirbek, M.A., Burghardt, N.S., Fenton, A.A., Dranovsky, A., and Hen, R. (2011). Increasing adult hippocampal neurogenesis is sufficient to improve pattern separation. Nature *472*, 466–470.

Sauer, J.F., Strüber, M., and Bartos, M. (2012). Interneurons provide circuit-specific depolarization and hyperpolarization. J. Neurosci. *32*, 4224–4229.

Scharfman, H.E. (1995). Electrophysiological evidence that dentate hilar mossy cells are excitatory and innervate both granule cells and interneurons. J. Neurophysiol. *74*, 179–194.

Schmidt-Hieber, C., Jonas, P., and Bischofberger, J. (2004). Enhanced synaptic plasticity in newly generated granule cells of the adult hippocampus. Nature *429*, 184–187.

Snyder, J.S., Kee, N., and Wojtowicz, J.M. (2001). Effects of adult neurogenesis on synaptic plasticity in the rat dentate gyrus. J. Neurophysiol. *85*, 2423–2431.

Song, J., Sun, J., Moss, J., Wen, Z., Sun, G.J., Hsu, D., Zhong, C., Davoudi, H., Christian, K.M., Toni, N., et al. (2013). Parvalbumin interneurons mediate neuronal circuitry-neurogenesis coupling in the adult hippocampus. Nat. Neurosci. *16*, 1728–1730.

Stone, S.S., Teixeira, C.M., Zaslavsky, K., Wheeler, A.L., Martinez-Canabal, A., Wang, A.H., Sakaguchi, M., Lozano, A.M., and Frankland, P.W. (2011). Functional convergence of developmentally and adult-generated granule cells in dentate gyrus circuits supporting hippocampus-dependent memory. Hippocampus *21*, 1348–1362.

Toni, N., Laplagne, D.A., Zhao, C., Lombardi, G., Ribak, C.E., Gage, F.H., and Schinder, A.F. (2008). Neurons born in the adult dentate gyrus form functional synapses with target cells. Nat. Neurosci. *11*, 901–907.

Torborg, C.L., Nakashiba, T., Tonegawa, S., and McBain, C.J. (2010). Control of CA3 output by feedforward inhibition despite developmental changes in the excitation-inhibition balance. J. Neurosci. *30*, 15628–15637.

Treves, A., Tashiro, A., Witter, M.P., and Moser, E.I. (2008). What is the mammalian dentate gyrus good for? Neuroscience *154*, 1155–1172.

Tronel, S., Fabre, A., Charrier, V., Oliet, S.H., Gage, F.H., and Abrous, D.N. (2010). Spatial learning sculpts the dendritic arbor of adult-born hippocampal neurons. Proc. Natl. Acad. Sci. USA *107*, 7963–7968.

Trouche, S., Bontempi, B., Roullet, P., and Rampon, C. (2009). Recruitment of adult-generated neurons into functional hippocampal networks contributes to updating and strengthening of spatial memory. Proc. Natl. Acad. Sci. USA *106*, 5919–5924.

van Praag, H., Schinder, A.F., Christie, B.R., Toni, N., Palmer, T.D., and Gage, F.H. (2002). Functional neurogenesis in the adult hippocampus. Nature *415*, 1030–1034.

Vivar, C., Potter, M.C., Choi, J., Lee, J.Y., Stringer, T.P., Callaway, E.M., Gage, F.H., Suh, H., and van Praag, H. (2012). Monosynaptic inputs to new neurons in the dentate gyrus. Nat. Commun. *3*, 1107.

Wiskott, L., Rasch, M.J., and Kempermann, G. (2006). A functional hypothesis for adult hippocampal neurogenesis: avoidance of catastrophic interference in the dentate gyrus. Hippocampus *16*, 329–343.

Zhao, C., Deng, W., and Gage, F.H. (2008). Mechanisms and functional implications of adult neurogenesis. Cell *132*, 645–660.